Tracking the Endocytic Pathway of Recombinant Protein Toxin Delivered by Multiwalled Carbon Nanotubes

Meiyan Wang, Shaoning Yu, Chuan Wang, and Jilie Kong*

Department of Chemistry and Institutes of Biomedical Sciences, Fudan University, Shanghai, P.R. China

ARTICLE

ABSTRACT The endocytic pathway of a recombinant protein toxin, ricin A-chain (RTA), delivered by multiwalled carbon nanotubes (MWCNTs) was tracked in HeLa cells by tagging RTA with enhanced green fluorescent protein (EGFP). EGFP—RTA was found to accumulate in the endosome and to be retrogradely transported to the endoplasmic reticulum, from which it translocated into the cytosol. Nuclear staining, *Z*-axis scanning with a laser scanning confocal microscope (LSCM), and transmission electron microscopy (TEM) indicated that the RTA exerted its toxic effects. Endocytosis-inhibiting tests with LSCM and flow cytometry showed that MWCNT—EGFP—RTA conjugates penetrated cells principally *via* clathrin-mediated endocytosis. These studies are beneficial to understanding the MWCNT-based intracellular drug delivery mechanism and provide guidelines for designing promising MWCNT-based vectors for targeting diagnostic or therapeutic compounds, not only to specific cells, but even to specific cellular compartments.

KEYWORDS: nanotubes · protein toxin · cancer cells · endocytic pathway · endoplasmic reticulum

Protein toxins have played a crucial role in cancer treatment.[1−3] As a potential anticancer member of the protein toxins family, ricin is identified as a class II ribosome-inactivating protein that is highly toxic to mammalian cells. Ricin consists of an enzymatic toxic domain, the A-chain (RTA), and a cell-binding domain, the B-chain (RTB), which are linked by a disulfide bond.[4] RTB binds to the receptors on the cell surface and transports RTA from the cell surface through the Golgi apparatus and toward the endoplasmic reticulum (ER) before its translocation to the cytosol, where RTA exerts the real toxic action by inactivating cell-free ribosomes, resulting in the inhibition of protein biosynthesis and apoptotic events.[3,5−9] Therefore, RTA cannot perform its cytotoxic function without assistance from a carrier, RTB, to traverse the cellular membrane.[10] Recently, recombinant immunotoxin has been employed in cancer therapy by using the antibody or other binding molecules to replace RTB;[11−14] however, the therapeutic uses of ricin immunotoxins have been limited by vascular leak syndrome, a side effect resulting from endothelial damage that causes fluid to escape from the bloodstream into the lungs, muscle, brain, and other tissues.[15−18] New drug delivery systems are required to deliver RTA to tumor cells.

During the past decade, nanoscale drug delivery systems rapidly progressed and are now being used in the pharmaceutical and biotechnology fields.[19,20] Among all nanomaterials, carbon nanotubes (CNTs) have been investigated as the most versatile candidates for such applications due to unique physical, chemical, and physiological properties, including large surface areas, high electrical conductivity, cell membrane penetrability, and versatile functionalization. Pioneer work by Dai groups and others have reported that CNTs could be used as efficient delivery vehicles to transport a wide range of molecules, such as peptides,[21] proteins,[22−24] nucleic acids,[25,26] therapeutic agents,[27,28] and vaccines[29] across membranes into living cells without the need for an external transporter. Because of their tubular structure and extremely high aspect ratio, functionalized CNTs with water solubility and biocompatibility can easily penetrate various biological barriers in mammals,[30] plants,[31] and microorganisms[32] while displaying low cytotoxicity.

In our previous work, recombinant RTA was found to be efficiently delivered into various cell lines (L-929, HL7702, MCF-7, HeLa, and COS-7), and then to perform highly cytotoxic functions, by multiwalled carbon nanotubes (MWCNTs) in the

*Address correspondence to jlkong@fudan.edu.cn.

Received for review June 25, 2010 and accepted October 14, 2010.

Published online October 26, 2010. 10.1021/nn101445y

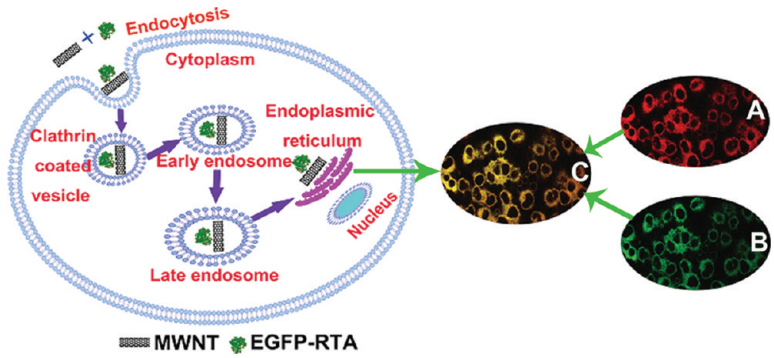

Figure 1. Schematic representation of EGFP−RTA delivered by multiwalled carbon nanotubes through the clathrin-mediated endocytosis pathway. MWCNT−EGFP−RTA conjugates arrived at the cell membrane, were engulfed by the cell membrane, and were subsequently internalized into cells inside endosomes and retrogradely transported to the endoplasmatic reticulum (ER). From the ER, the conjugates were translocated to the cytosol to exert their toxic effects. (A) ER-Tracker Blue-White DPX fluorescence images. (B) EGFP confocal fluorescence images. (C) Overlap of confocal fluorescence images B and C in HeLa cells.

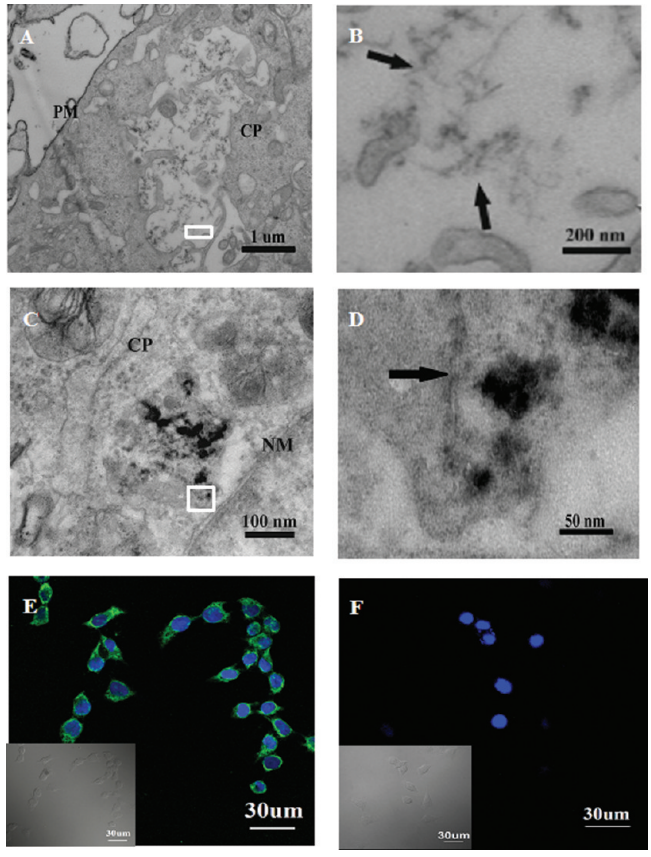

Figure 2. The distribution of MWCNT-RTA conjugates inside HeLa cells. TEM images of (A) MWCNT−RTA conjugates entrapped in the peripheral cytoplasm of HeLa cells, (B) a magnification of the white rectangle in panel A, (C) MWCNT−RTA conjugates moving inward at perinuclear regions of HeLa cells, and (D) a magnification of the white boxed area in panel C. PM, plasma membrane; CP, cytoplasm; NM, nuclear membrane. The black arrows indicate individual short MWCNTs within a cell. (E) Confocal microscopy images of cells after incubation with MWCNT−RTA conjugates. (F) Cells after incubation with 1.0 μM RTA alone (no MWCNTs present). The insets show the optical images of cells within the areas. The localization was determined by indirect immunofluorescence using a primary antibody against His-tag and FITC-conjugated antirabbit secondary antibody. Nuclei were counterstained with DAPI (4′,6-diamidino-2-phenylindole). [MWCNTs] = 25 μg/mL, [RTA] = 1.0 μM.

absence of RTB.[24] Thus far, the intracellular pathway of RTA transportation by MWCNTs is not clear. Tracking the pathway of the protein toxins inside cells will help us further understand some key factors in cellular drug delivery, including how they enter cells, where they distribute and locate to, and when they begin to function. In this study, enhanced green fluorescent protein (EGFP) was fused to RTA to visualize its roadmap in a single cell. Noncovalently bound MWCNT−EGFP−RTA conjugates were prepared to demonstrate the panoramic view of the endocytic translocation of RTA. The dynamic uptake process of the MWCNT−EGFP−RTA conjugates, including the mobility and transport pathway, were fully tracked in a single HeLa cell using laser scanning confocal microscopy (LSCM), transmission electron microscopy (TEM), and flow cytometry (FCM).

Although several possible mechanisms have been proposed for cell internalization of CNTs, the exact mechanism of cellular binding and the dynamic fate of the internalized CNTs continues to raise significant debate. Kam *et al.*[33] and Heller *et al.*[34,35] reported that protein- or DNA-coated single-walled carbon nanotubes (SWCNTs) can enter cells *via* energy-dependent endocytosis, whereas Kostarelos[36] and Bianco and Prato[21] proposed an energy-independent nonendocytotic pathway, termed the nanoneedle mechanism, involving the insertion and diffusion of SWCNTs and MWCNTs across different cell membranes. In addition, Porter *et al.*[37] and Cherukuri *et al.*[38] reported the cellular uptake of SWCNTs by macrophages. The large discrepancy between different studies could be due partly to the lack of enough molecular proof of conjugate migration, as well as the different surface modifications of CNTs. In addition, most of the reported experiments were carried out on SWCNTs wrapped with a variety of biomolecules. However, little is known about the intracellular dynamic fate of the internalized MWCNTs. In our work, the cellular uptake of RTA-mediated by MWCNTs is predominately through the clathrin-mediated endocytosis pathway, which differs from the majority of published data showing MWCNT uptake by living cells through an energy-independent nonendocytotic mechanism.[21] Here, we show for the first time that MWCNT−EGFP−RTA conjugates accumulate in the endosome and retrogradely transport to the ER after endocytosis (Figure 1). The intracellular endocytic pathway of the conjugates in living cells definitely reflected the delivery capability of MWCNTs for RTA targeting to the ER, which is necessary for the toxins to reach the cytosol where they exert their intrinsic toxic effects.[39] We believe that the molecular elucidation presented here may provide more knowledge regarding the intracellular endocytic mechanism and result in more opportuni-

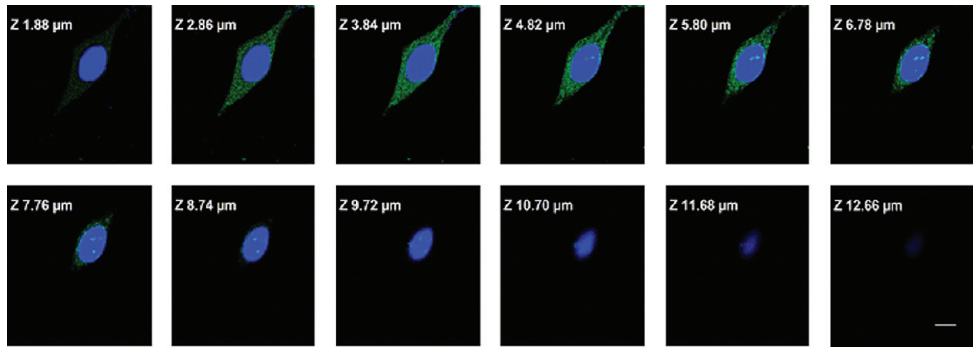

Figure 3. Different *Z*-axis confocal images of MWCNT−EGFP−RTA conjugates taken up by HeLa cells. The cells were grown on chamber slides and incubated in culture medium supplemented with MWCNT−EGFP−RTA conjugates ([MWCNTs] = 25 μg/mL, [EGFP-RTA] = 1.0 μM) for 22 h. The cells were washed and analyzed with a 60× oil immersion objective (numerical aperture = 1.4) along their *Z*-axis at 0.19 μm intervals using confocal microscopy. The 12 slides represent the same HeLa cell scanned from the dish bottom to the top of the cell. The cell nuclei and cytosol are stained with blue (DAPI) and green (EGFP), respectively. The scale bar represents 10 μm.

ties for the design of highly specific and efficient delivery systems for therapeutic treatment.

RESULTS AND DISCUSSION

Preliminary Studies on Tracking MWCNT-RTA Conjugates. Noncovalently bound MWCNT conjugates were prepared by mixing the protein with cut acid-oxidized MWCNTs by electrostatic interactions and π−π stacking (for the details of all experiments, see Supporting Information). To track MWCNT−RTA conjugates, TEM and LSCM were used to observe the distribution of conjugates inside the cells. TEM images of fixed cells showed that RTA was internalized by MWCNTs into the peripheral (Figure 2A,B) and perinuclear cytoplasm (Figure 2C,D). The green fluorescence signal was predominately observed under confocal microscopy in the cytoplasm of the cells treated with the MWCNT-RTA conjugates (Figure 2E, single channel images shown in Supplementary Figure 4A), which is consistent with our TEM observations. In contrast, no obvious fluorescence was observed for HeLa cells treated with the same concentration of free RTA (Figure 2F, single channel images shown in Supplementary Figure 4B). The results strongly indicated that MWCNTs are responsible for the transportation of the protein toxin in cells and to the cytoplasm where RTA performed its biological function, because RTA is generally nontoxic outside the cell due to its low efficiency at entering cells by itself. RTA enters cancer cells with the help of MWCNTs and exerts its cytotoxic functions.

Intracellular Trafficking of RTA Delivered by MWCNTs. Knowing that the intracellular trafficking of RTA is critical to obtaining a full understanding of its function, EGFP was fused to external RTA, which does not influence RTA biological activity (Supplementary Figure 3). GFP and its homologues are widely used as fluorescent markers to track protein behavior in live cells.[40,41] Therefore, as noted above, the intracellular uptake of MWCNT−EGFP−RTA conjugates in a single live cell was further investigated by confocal microscopy. Using *Z*-axis fluorescent microscopy and three-dimensional image reconstruction, we studied the spatial distribution of the MWCNT−EGFP−RTA conjugates after incubation with HeLa cells. This differential uptake of conjugates by HeLa cells was reproducibly observed with the different passages of cells. Combined with DAPI staining, optical confocal microscopy sections of a single living cell revealed that the green fluorescence was mainly localized within the cytoplasm (Figure 3, single channel images in Supplementary Figure 5A and video 001). The data demonstrate that MWCNT−EGFP−RTA conjugates were largely internalized into the cytoplasm fraction of HeLa cells. In contrast, few of the EGFP−RTA conjugates were visualized inside the cells (Supplementary Figure 6). It is clear that the EGFP−RTA delivered by MWCNTs are distributed in the cytoplasm, where RTA confers cellular toxicity by

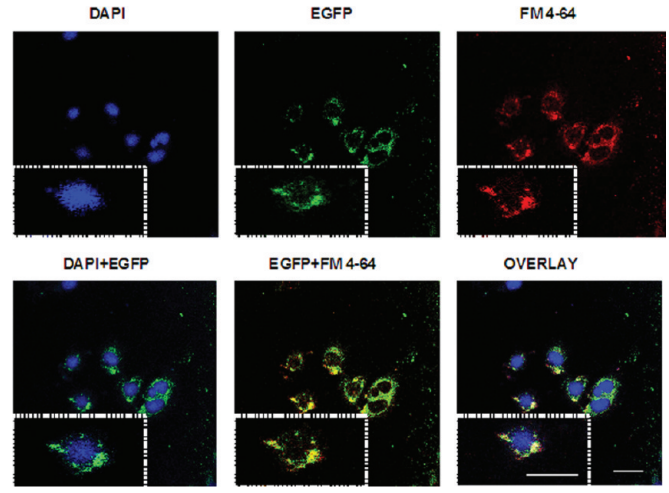

Figure 4. Intracellular location of MWCNT−EGFP−RTA conjugates in HeLa cells. The internalization of MWCNT−EGFP−RTA conjugates was determined by confocal images of cells after incubation with MWCNT−EGFP−RTA conjugates ([MWCNTs] = 25 μg/mL, [EGFP−RTA] = 1.0 μM) for 10 h in the presence of FM 4−64, a red membrane and endocytotic vesicle marker. The images identify areas of green EGFP−RTA proteins and red FM 4-64 colocalization (yellow). The inset shows a magnification of a single cell in the areas. The scale bar represents 30 μm.

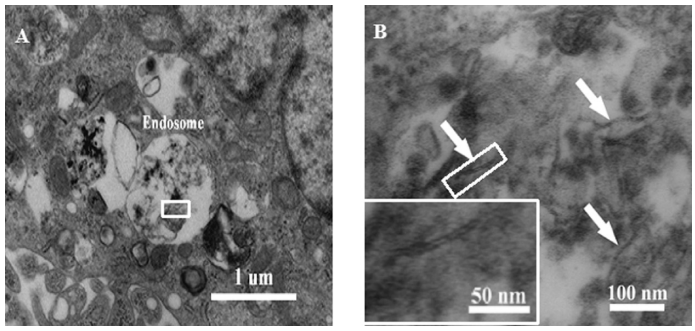

Figure 5. TEM characterization of the subcellular localization of MWCNT−RTA conjugates in HeLa cells. (A) MWCNT bundles localized in the endosome. (B) Magnification of the white rectangle in A. The inset shows a magnification of the individual short MWCNTs in the white rectangle in B. The white arrows indicate individual short MWCNTs within the endosome. [MWCNTs] = 25 μg/mL, [RTA] = 1.0 μM.

catalytically inactivating ribosomes and leading to rapid inhibition of protein synthesis and cell death.

Endosomal Accumulation of MWCNT−EGFP−RTA Conjugates. Ricin can be taken up by energy-mediated endocytosis.[4] We used confocal microscopy to investigate whether the endocytosis and intracellular trafficking of MWCNT−EGFP−RTA conjugates were similar to that of ricin itself. As shown in Figure 4, after a 10 h incubation, MWCNT−EGFP−RTA conjugates internalized inside mammalian cells displayed good overlap with the red endocytosis endosome marker FM 4-64, which enters endomembrane organelles, including the vacuole, Golgi, and ER *via* the endocytotic pathway. These data provide direct evidence for the endocytosis of MWCNT−EGFP−RTA conjugates. The conjugates accumulated in the endosome after internalization and avoided degradation inside the intracellular compartments. Our findings are also consistent with previously reported data that natural ricin is taken up into the cell in clathrin-coated vesicles by receptor-mediated endocytosis, and from there it is delivered to the endosomal network.[9]

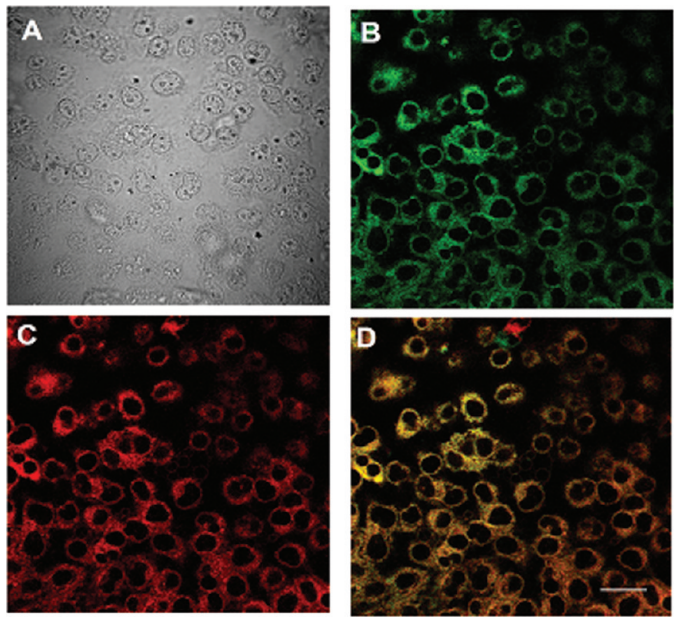

Figure 6. MWCNT−EGFP−RTA conjugates located in the ER of HeLa cells after incubation for 22 h. The green fluorescence signal from intracellular MWCNT−EGFP−RTA overlapped with the signal from the ER stained with ER-Tracker Blue-White DPX. The overlapped portion appears in yellow. (A) brightfield images; (B) EGFP fluorescence images; (C) ER-Tracker Blue-White DPX fluorescence images; (D) overlap of fluorescence images B and C. Scale bar = 30 μm, [MWCNTs] = 25 μg/mL, [EGFP−RTA] = 1.0 μM.

The confocal fluorescence microscope can only observe the internalization of fluorescence-labeled CNTs into cells; however, tracing the same process with unlabeled CNTs, such as single nanotubes, is challenging. Here, we directly track the distribution of unstained MWNT−RTA conjugates into cells using TEM. As shown in Figure 5A, bundled MWCNTs carrying RTA localized in the endosomes. Subsequent magnifications (Figure 5B) provide a higher-resolution view of the intracellular localization of the MWNT−RTA conjugates. Here, we directly visualized individual MWCNTs in the endosomes, where the endocytotic uptake of the hollow nanotubes indeed occurred, consistent with the results from fluorescence confocal microscopy.

Transport of MWCNT−EGFP−RTA Conjugates to the Endoplasmic Reticulum. Ricin has been reported to enter cells by endocytic routing from endosomes and into the Golgi apparatus, and further retrogradely transported to the ER. From the ER, ricin is translocated into the cytosol to exert its toxic effect.[42] However, RTA does not penetrate the ER membrane directly.[39] Some investigations have suggested that RTA reaches the ER and takes advantage of a quality control pathway, termed ER-associated protein degradation (ERAD), to reach the cytosol.[43] Another study supported that RTA must make specific interactions with ER components to accomplish the unfolding that is required for translocation to the cytosol.[44] To target ribosomes in the mammalian cytosol, RTA must first negotiate the endomembrane system of the cell to reach the ER. In our study, after exposure of the cells to EGFP−RTA or MWCNT−EGFP−RTA conjugates for 22 h, EGFP−RTA was visualized as overlapping with ER-Tracker Blue-White DPX using LSCM (Figure 6 and Supporting Information video 002). In contrast, few of the endocytic EGFP−RTA were visualized inside the cells (Supplementary Figure 7). These results provide the first direct evidence that the endocytosed EGFP−RTA fusion protein delivered by MWCNTs is retrogradely transported to the ER, indicating that the ER might be a final organelle for RTA translocation.

To directly visualize the intracellular trafficking of MWCNT−RTA conjugates, we also tracked the same process of MWCNT−RTA conjugates entering cells using TEM. Figure 7 illustrates the different stages of the endocytosis process. After being endocytosed, some MWCNTs are visualized near the Golgi apparatus (Figure 7A,B) and ER (Figure 7C). The accumulation of some MWCNTs in the ER is consistent with the confocal fluorescence microscopy results (Figure 7D). Our observations indicated that MWCNT bundles retrogradely trans-

port the protein to the ER, which was the most possible route for their cellular fate and similar to that of ricin itself. In our experiment, RTB was substituted by MWCNTs and similar translocation of RTA appeared to occur, which suggests that MWCNTs could become novel efficient transporters of RTA.

Cellular Uptake Mechanism of MWCNT−EGFP−RTA Conjugates. To further investigate the possible mechanism for MWCNT−EGFP−RTA conjugate entry into cells, we studied the effect of energy depletion on its cellular uptake. Endocytosis is known to be a general entry mechanism for various extracellular materials and is an energy-dependent process. ATP production is disrupted when cells are cultured at 4 °C or with NaN_3.[33] Cellular incubations with MWCNT−EGFP−RTA conjugates were carried out at 4 and 37 °C with NaN_3. Very weak green fluorescence was seen in the cells cultured at 4 and 37 °C with NaN_3 (Figure 8A,B) compared to the control (Figure 8C) using confocal microscopy. This finding was further quantitatively confirmed using FCM measurements (Figure 8D, for the original data see Supplementary Figure 8), indicating that the cellular uptake of MWCNT−EGFP−RTA conjugates is an active transport process requiring energy. These phenomena are in good agreement with an energy-dependent endocytotic mechanism.

Several possible endocytic processes exist for internalizing materials, such as clathrin-mediated endocytosis, caveolae-mediated endocytosis, and clathrin-caveolae-independent endocytosis. To determine the precise endocytotic pathway involved in the internalization of MWCNT−EGFP−RTA conjugates, we tested whether specific endocytotic inhibitors[45] block the internalization using confocal microscopy and FCM. As shown in Figure 9, green fluorescent signal inside the cells is very weak when the cells are pretreated with chlorpromazine (Figure 9B). However, the cells pretreated with nystatin (Figure 9C) or cytochalasin D (Figure 9D) expressed obvious green fluorescence at basically the same level as control cells (Figure 9A). FCM was used to quantify the inhibitory effects based on the reduction in fluorescence compared to the control. The FCM data also showed that the fluorescence intensity was blocked to the background level (cell only) when chlorpromazine was introduced into the cell culture, but the green fluorescence intensity was similar to the normal cells cultured at 37 °C. These data are consistent with the result from confocal fluorescence microscopy (Figure 9E, for the original data see Supplementary Figure 9). These results indicate that the internalization of MWCNT−EGFP−RTA conjugates was obviously inhibited by chlorpromazine, which is a cationic amphiphilic drug that prevents clathrin-mediated endocytosis by disrupting the assembly of the clathrin adaptor protein at the cell surface, but nystatin and cytochalasin D did not have an inhibitory effect. Altogether, we concluded that MWCNT−EGFP−RTA conjugates were

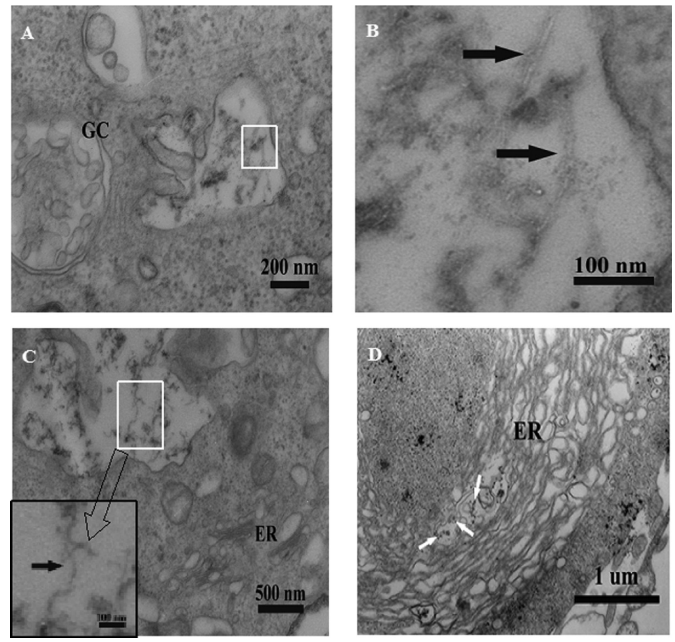

Figure 7. TEM images capturing the endocytosis of MWCNT−RTA conjugates into HeLa cells. (A) MWCNT bundles localized near the Golgi complex (GC). (B) Magnification of the white rectangle in panel A. (C) MWCNT bundles localized near the endoplasmic reticulum (ER). The inset shows a magnification of individual short MWCNTs in the white rectangle. (D) MWCNT bundles accumulated in the ER. [MWCNTs] = 25 μg/mL, [RTA] = 1.0 μM. The black arrows indicate individual short MWCNTs within the subcellular organelle; white arrows indicate aggregates of MWCNTs within the ER.

internalized into HeLa cells principally *via* clathrin-mediated endocytosis. Our findings are also consistent with data reported by Shi Kam *et al.*, Jin *et al.*, and Heller *et al.*, who reported that energy-dependent endocytosis is the internalization mechanism used by SWCNTs to carry various types of other biological molecules into cells.[21,22,25] However, our results clearly differ from the majority of published data in that MWCNTs are taken up by living cells through an energy-independent nonendocytotic pathway that involves the insertion and diffusion of nanotubes across cell membranes. The discrepancy in uptake mechanisms might be due to different molecular loadings on the CNTs and/or different experimental procedures. This work extends the current understanding of the intracellular behavior and uptake mechanism of carbon nanotube transporters for biological delivery applications.

CONCLUSION

We have shown that a recombinant protein toxin, RTA, was internalized into the cytoplasm where it can exert a direct toxic effect, and investigated the endocytic pathway of the delivery of the protein by MWCNTs. MWCNT−EGFP−RTA conjugates are reported to be taken up by HeLa cells *via* a clathrin-mediated endocytosis mechanism, which differs from the majority of published data showing that MWCNTs are taken up by living cells through an energy-

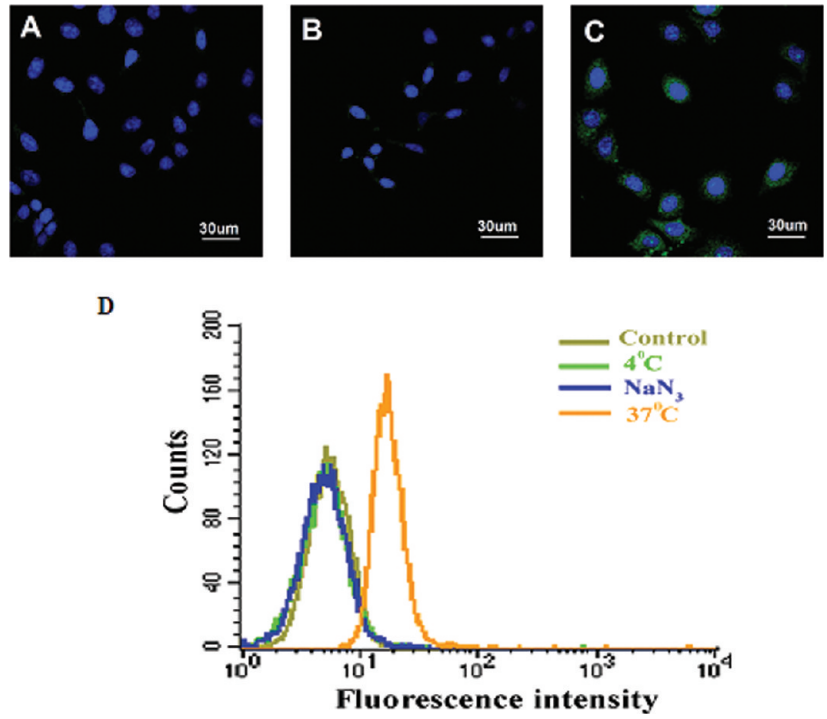

Figure 8. Energy-dependent cell uptake of MWCNT−EGFP−RTA conjugates. Confocal microscopy images of HeLa cells after incubation with MWCNT−EGFP−RTA conjugates ([MWCNTs] = 25 μg/mL, [EGFP−RTA] = 1.0 μM) at (A) 4 °C, (B) after pretreatment with NaN_3, and (C) at 37 °C. The cell nuclei and cytosol are stained blue (DAPI) and green (EGFP), respectively. (D) Flow cytometry analysis after incubation with MWCNT−EGFP−RTA for untreated cells, cells pretreated with sodium azide, and cultured at 4 °C instead of 37 °C. The dark yellow line corresponds to control cells, the green line corresponds to cells cultured at 4 °C, the blue line corresponds to cells pretreated with sodium azide, and the orange line corresponds to cells cultured at 37 °C. Each treatment was made in triplicate.

independent nonendocytotic pathway that involves the insertion and diffusion of nanotubes across cell membranes. To the best of our knowledge, this is the first time MWCNT−EGFP−RTA conjugates have been directly visualized to accumulate in the endosome after endocytosis and retrogradely transported to the ER, where they are translocated to the cytosol to exert their toxic effects. Therefore, a better understanding of the mechanisms of cell entry, trafficking, and toxicity of these model delivery vectors will provide both opportunities and challenges for designing more specific and efficient systems for therapeutic targeting.

EXPERIMENTAL PROCEDURES

Materials. MWCNTs (purity > 90%, length > 1 μm, diameter < 10 nm) were purchased from Nanotech Port Co., Ltd. (Shenzhen, China). Bovine serum albumin (BSA, 66 kD) was purchased from Chemical Reagent Company (Shanghai, China). Chlorpromazine was obtained from Sine JiuFu Pharmaceutical Company (Shanghai, China). Cytochalasin and D nystatin was purchased from Shanghai Solarbio Bioscience & Technology Co., Ltd. (Shanghai, China). All tissue culture materials were obtained from Invitrogen, and the other reagents (analytical grade) were purchased from Sigma-Aldrich (St. Louis, MO).

Preparation of Cell Sections for TEM Analysis. HeLa cells (1.25×10^5) were cultured in Dulbecco's minimal essential medium (DMEM) in a 6-well plate at 37 °C in the presence of 5% CO_2 until 75% confluent. The cells were then incubated with a solution of MWCNT−RTA in phosphate-buffered saline (PBS) for 22 h, fixed by 2.5% glutaraldehyde in 0.1 M PBS (pH 7.2) for 2 h, washed three times with 0.1 M PBS (15 min each wash), and then treated with a 1% OsO_4 solution in cacodilate buffer for 2−3 h at room temperature. Cells were carefully rinsed with 0.1 M PBS. After several washes, the cells were dried by treating with 50%, 70%, 90% ethanol, a mixture of 90% ethanol and acetone (1:1, v/v), and 90% acetone for 15 min each at 4 °C, and then three times with absolute acetone for 20 min at room temperature. The specimen was then embedded in an epoxy resin by treating with absolute acetone and embedding solution (2:1, v/v) for 2−3 h at room temperature, absolute acetone and embedding solution (1:2, v/v) overnight at room temperature, and absolute embedding solution for 2−3 h at 37 °C. The specimen was stored in an oven overnight at 37 °C, 45 °C for 12 h, and 60 °C for 24 h. Specimens were then subsequently sectioned into 50 to 60-nm-thick slices with an LKB-I ultramicrotome. Selected sections were stained with uranyl acetate and lead citrate and observed with a Philips CM120 transmission electron microscope with an accelerating voltage of 120 kV.

Immunofluorescence Analysis. HeLa cells were cultured directly onto glass coverslips using DMEM medium supplemented with 10% FBS and 1% penicillin−streptomycin to allow 70% confluency in 24 h at 37 °C. After the cells were incubated with RTA and MWCNT-RTA conjugates in a 6-well plate for 22 h at 37 °C, the cell medium was removed and the cells were washed with PBS and fixed for 10 min with ice-cold acetone. Cells were subsequently washed three times in PBS and then blocked with 10% goat serum in PBS for 20 min before being incubated with primary antibody (rabbit anti-His, 1:1000 in blocking buffer) for 2 h at 37 °C. The cells were washed with three changes of PBS for 5 min each before incubating with FITC-labeled secondary antirabbit antibody (1:100 in blocking buffer, Sigma) in the dark for 1 h. The cells were washed three times for 5 min each with PBS, counterstained with DAPI (0.25 μg/mL, Molecular Probes) for 10

min, rinsed with PBS three times for 15 min, and the coverslips transferred onto microscope slides and fixed with mounting medium to be visualized by LSCM (Olympus FV1000) using oil immersion at 60× magnification.

LSCM of Living Cells Incubated with MWCNT−EGFP−RTA Conjugates. HeLa cells were plated in 35-mm glass bottom culture dishes, grown to 80% confluency for 24 h at 37 °C, and washed three times with prewarmed PBS. The culture medium was then replaced with serum-free medium (SFM) mixed with MWCNT−EGFP−RTA conjugates for 22 h at 37 °C. After incubation, the cell medium was removed from the chambered cover slides and washed with PBS three times. The cells were counterstained with DAPI for 10 min, rinsed with PBS three times for 15 min, and replaced with SFM. HeLa cells were imaged directly on the chambered cover glass using LSCM (Olympus FV1000, BX61W1) and a 60× oil immersion objective lens. Individual images were taken along the *Z*-axis of internalized MWCNT−EGFP−RTA conjugates in HeLa cells at 0.19 μm intervals from the dish bottom to the top of the cell. Images were combined and deconvoluted to reconstruct a three-dimensional image of the cells for additional analysis.

LSCM of the Subcellular Localization of MWCNT−EGFP−RTA Conjugates. HeLa cells grew on coverslips inside a Petri dish filled with DMEM medium containing 10% FBS and 1% penicillin−streptomycin to allow 70% confluency in 24 h at 37 °C. The medium was removed from the dish and high glucose DMEM medium containing 0.45% glucose was added, as well as 1.0 μM EGFP−RTA or MWCNT−EGFP−RTA conjugates on the control slides and treated slides, respectively. The slides were incubated at 37 °C for 10 or 22 h. The slides were washed with HBSS (with Ca^{2+} and Mg^{2+}) three times.

For FM 4-64 staining, FM 4-64 (5 μM, Molecular Probes) was added to cells and then incubated for 10−15 min at 30 °C with shaking. For ER-Tracker Blue-White DPX staining, the medium was removed from the dish and prewarmed ER-Tracker Blue-White DPX-containing high glucose DMEM medium (1 μM) added. The cells were incubated for approximately 0.5 h under growth conditions. The slides were washed with HBSS (with Ca^{2+} and Mg^{2+}) three times and observed using LSCM. The absorption of EGFP was 488 nm, and the peak fluorescence emission ranged from 500 to 600 nm. The absorption of the FM 4-64 dye was 558 nm, and the peak fluorescence emission was monitored from 650 to 750 nm. The absorption of ER-Tracker Blue-White DPX was 405 nm, and the peak fluorescence emission ranged from 425 to 475 nm.

Endocytosis Inhibition. HeLa cells were first pretreated with one of the endocytosis inhibitors (10 mM sodium azide for depletion of ATP; 10 μg/mL chlorpromazine as an inhibitor of clathrin-mediated endocytosis; 15 μg/mL nystatin as an inhibitor of caveolae-mediated endocytosis; and 1 μg/mL cytochalasin D as an inhibitor of macropinocytosis) in FBS-free DMEM for 1 h, and then incubated with MWCNT−EGFP−RTA conjugates for another 22 h. The cells were cultured at 4 °C, instead of the regular 37 °C conditions. After incubation, the cells were rinsed three times with 0.01 M PBS prior to examination by LSCM.

Quantitative Study of Uptake by FCM. The cells were seeded in 6-well plates at a density of 2.5×10^5 cells per well and incubated in DMEM cell culture media for 24 h at 37 °C and 5% CO_2. Then the cells were incubated with MWCNT−EGFP−RTA conjugates and control at 37 °C for 22 h. After incubation, the cells were detached using trypsin, centrifuged at 1000*g* for 10 min, and analyzed using a Becton Dickinson FACSCalibur flow cytometer. A total of 1×10^5 cells were collected and analyzed for each sample. Three replicates were done for each sample.

Acknowledgment. This work was supported by the NSFC (Grant Nos. 20890022, 20945001, 30970631), Shanghai Leading Academic Discipline Project B109 and Shanghai governmental funds 08XD14009 and 09PJD007.

Supporting Information Available: Supplementary Figures 1−9 and videos 001 and 002. This material is available free of charge *via* the Internet at http://pubs.acs.org.

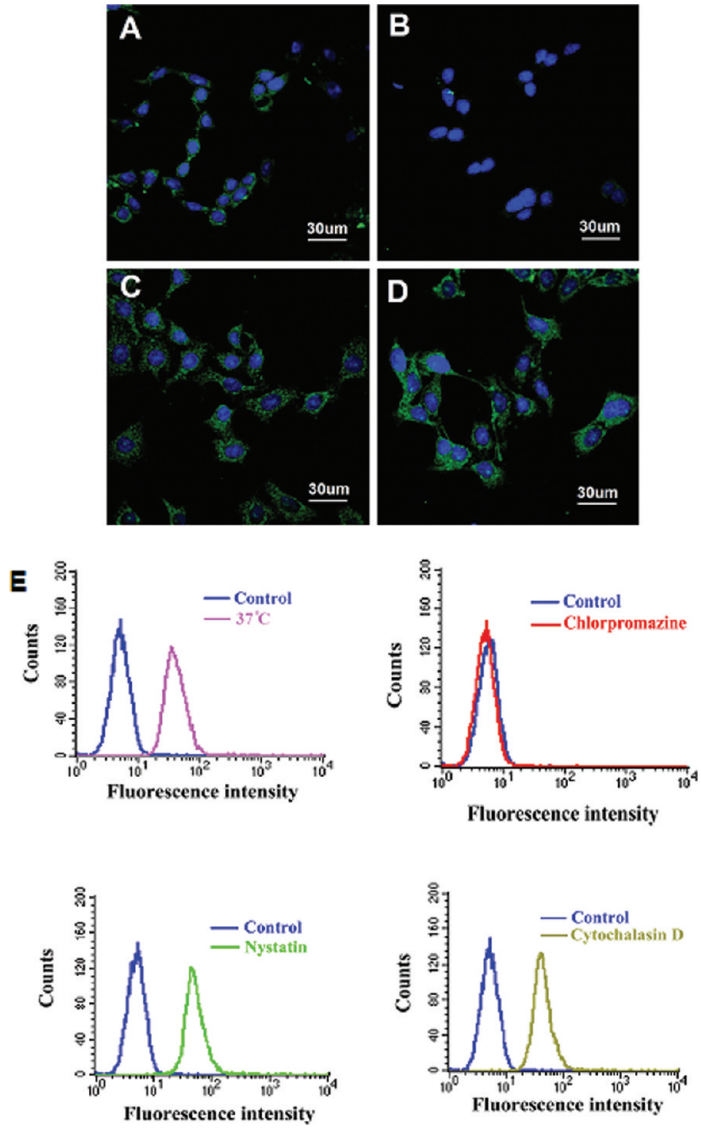

Figure 9. Internalization in the presence of endocytotic inhibitors. Confocal microscope images of (A) control cells and (B) cells incubated for 60 min with 10 μg/mL chlorpromazine, which inhibits clathrin-mediated endocytosis, (C) 15 μg/mL nystatin, which inhibits caveolae-mediated endocytosis, or (D) 1 μg/mL cytochalasin D, which inhibits macropinocytosis, prior to incubation with the MWCNT−EGFP−RTA conjugates. (E) Flow cytometry analysis of cells after incubation with MWCNT−EGFP−RTA conjugates without pretreatment (control) and cells pretreated with chlorpromazine, nystatin, or cytochalasin D. [MWCNTs] = 25 μg/mL, [EGFP−RTA] = 1.0 μM. Each treatment was made in triplicate.

REFERENCES AND NOTES

1. Fitzgerald, D. J. P.; Padmanabhan, R.; Pastan, I.; Willingham, M. C. Adenovirus-Induced Release of Epidermal Growth-Factor and Pseudomonas Toxin into the Cytosol of KB-Cells During Receptor-Mediated Endocytosis. *Cell* **1983**, *32*, 607–617.
2. Pastan, I.; Willingham, M. C.; Fitzgerald, D. J. P. Immunotoxins. *Cell* **1986**, *47*, 641–648.
3. Johannes, L.; Decaudin, D. Protein Toxins: Intracellular Trafficking for Targeted Therapy. *Gene Ther.* **2005**, *12*, 1360–1368.
4. Sandvig, K.; van Deurs, B. Entry of Ricin and Shiga Toxin into Cells: Molecular Mechanisms and Medical Perspectives. *Embo J.* **2000**, *19*, 5943–5950.
5. Jaffrezou, J. P.; Levade, T.; Thurneyssen, O.; Chiron, M.; Bordier, C.; Attal, M.; Chatelain, P.; Laurent, G. *In Vitro* and *in Vivo* Enhancement of Ricin-A Chain Immunotoxin

Activity by Novel Indolizine Calcium-Channel Blockers-Delayed Intracellular Degradation Linked to Lipidosis Induction. *Cancer Res.* **1992**, *52*, 1352–1359.
6. Rapak, A.; Falnes, P. O.; Olsnes, S. Retrograde Transport of Mutant Ricin to the Endoplasmic Reticulum with Subsequent Translocation to Cytosol. *Proc. Natl. Acad. Sci. U.S.A.* **1997**, *94*, 3783–3788.
7. Sandvig, K.; van Deurs, B. Transport of Protein Toxins into Cells: Pathways Used by Ricin, Cholera Toxin, and Shiga Toxin. *FEBS Lett.* **2002**, *529*, 49–53.
8. Sandvig, K.; van Deurs, B. Membrane Traffic Exploited by Protein Toxins. *Annu. Rev. Cell Dev. Biol.* **2002**, *18*, 1–24.
9. Watson, P.; Spooner, R. A. Toxin Entry and Trafficking in Mammalian Cells. *Adv. Drug Delivery Rev.* **2006**, *58*, 1581–1596.
10. Spooner, R. A.; Watson, P. Drug Targeting: Learning from Toxin Entry and Trafficking in Mammalian Cells. *Curr. Opin. Drug Discovery Dev.* **2010**, *13*, 86–95.
11. Kreitman, R. J. Recombinant Toxins for the Treatment of Cancer. *Curr. Opin. Mol. Ther.* **2003**, *5*, 44–51.
12. Olsnes, S. The History of Ricin, Abrin and Related Toxins. *Toxicon* **2004**, *44*, 361–370.
13. Leshin, J.; Danielsen, M.; Credle, J. J.; Weeks, A.; O'Connell, K. P.; Dretchen, K. Characterization of Ricin Toxin Family Members from Ricinus Communis. *Toxicon* **2010**, *55*, 658–661.
14. Pastan, I.; Hassan, R.; FitzGerald, D. J.; Kreitman, R. J. Immunotoxin Therapy of Cancer. *Nat. Rev. Cancer* **2006**, *6*, 559–565.
15. Baluna, R.; Rizo, J.; Gordon, B. E.; Ghetie, V.; Vitetta, E. S. Evidence for a Structural Motif in Toxins and Interleukin-2 That May Be Responsible for Binding to Endothelial Cells and Initiating Vascular Leak Syndrome. *Proc. Natl. Acad. Sci. U.S.A.* **1999**, *96*, 3957–3962.
16. Baluna, R.; Coleman, E.; Jones, C.; Ghetie, V.; Vitetta, E. S. The Effect of a Monoclonal Antibody Coupled to Ricin A Chain-Derived Peptides on Endothelial Cells *in Vitro*: Insights into Toxin-Mediated Vascular Damage. *Exp. Cell Res.* **2000**, *258*, 417–424.
17. Sturm, M. B.; Roday, S.; Schramm, V. L. Circular DNA and DNA/RNA Hybrid Molecules as Scaffolds for Ricin Inhibitor Design. *J. Am. Chem. Soc.* **2007**, *129*, 5544–5550.
18. Kreitman, R. J. Taming Ricin Toxin. *Nat. Biotechnol.* **2003**, *21*, 372–374.
19. Cho, K. J.; Wang, X.; Nie, S. M.; Chen, Z.; Shin, D. M. Therapeutic Nanoparticles for Drug Delivery in Cancer. *Clin. Cancer Res.* **2008**, *14*, 1310–1316.
20. Farokhzad, O. C.; Langer, R. Impact of Nanotechnology on Drug Delivery. *ACS Nano* **2009**, *3*, 16–20.
21. Pantarotto, D.; Briand, J. P.; Prato, M.; Bianco, A. Translocation of Bioactive Peptides across Cell Membranes by Carbon Nanotubes. *Chem. Commun.* **2004**, 16–17.
22. Kam, N. W. S.; Jessop, T. C.; Wender, P. A.; Dai, H. J. Nanotube Molecular Transporters: Internalization of Carbon Nanotube−Protein Conjugates into Mammalian Cells. *J. Am. Chem. Soc.* **2004**, *126*, 6850–6851.
23. Kam, N. W. S.; Dai, H. J. Carbon Nanotubes as Intracellular Protein Transporters: Generality and Biological Functionality. *J. Am. Chem. Soc.* **2005**, *127*, 6021–6026.
24. Weng, X. X.; Wang, M. Y.; Ge, J.; Yu, S. N.; Liu, B. H.; Zhong, J.; Kong, J. L. Carbon Nanotubes as a Protein Toxin Transporter for Selective HER2-Positive Breast Cancer Cell Destruction. *Mol. Biosyst.* **2009**, *5*, 1224–1231.
25. Liu, Y.; Wu, D. C.; Zhang, W. D.; Jiang, X.; He, C. B.; Chung, T. S.; Goh, S. H.; Leong, K. W. Polyethylenimine-Grafted Multiwalled Carbon Nanotubes for Secure Noncovalent Immobilization and Efficient Delivery of DNA. *Angew. Chem., Int. Ed.* **2005**, *44*, 4782–4785.
26. Cai, D.; Mataraza, J. M.; Qin, Z. H.; Huang, Z. P.; Huang, J. Y.; Chiles, T. C.; Carnahan, D.; Kempa, K.; Ren, Z. F. Highly Efficient Molecular Delivery into Mammalian Cells Using Carbon Nanotube Spearing. *Nat. Methods* **2005**, *2*, 449–454.
27. Bianco, A.; Kostarelos, K.; Partidos, C. D.; Prato, M. Biomedical Applications of Functionalised Carbon Nanotubes. *Chem. Commun.* **2005**, 571–577.
28. Allen, T. M.; Cullis, P. R. Drug Delivery Systems: Entering the Mainstream. *Science* **2004**, *303*, 1818–1822.
29. Panhuis, M. I. H. Vaccine Delivery by Carbon Nanotubes. *Chem. Biol.* **2003**, *10*, 897–898.
30. Qu, G. B.; Bai, Y. H.; Zhang, Y.; Jia, Q.; Zhang, W. D.; Yan, B. The Effect of Multiwalled Carbon Nanotube Agglomeration on Their Accumulation in and Damage to Organs in Mice. *Carbon* **2009**, *47*, 2060–2069.
31. Liu, Q. L.; Chen, B.; Wang, Q. L.; Shi, X. L.; Xiao, Z. Y.; Lin, J. X.; Fang, X. H. Carbon Nanotubes as Molecular Transporters for Walled Plant Cells. *Nano Lett.* **2009**, *9*, 1007–1010.
32. Kang, S.; Herzberg, M.; Rodrigues, D. F.; Elimelech, M. Antibacterial Effects of Carbon Nanotubes: Size Does Matter. *Langmuir* **2008**, *24*, 6409–6413.
33. Kam, N. W. S.; Liu, Z. A.; Dai, H. J. Carbon Nanotubes as Intracellular Transporters for Proteins and DNA: An Investigation of the Uptake Mechanism and Pathway. *Angew. Chem., Int. Ed.* **2006**, *45*, 577–581.
34. Jin, H.; Heller, D. A.; Strano, M. S. Single-Particle Tracking of Endocytosis and Exocytosis of Single-Walled Carbon Nanotubes in NIH-3T3 Cells. *Nano Lett.* **2008**, *8*, 1577–1585.
35. Jin, H.; Heller, D. A.; Sharma, R.; Strano, M. S. Size-Dependent Cellular Uptake and Expulsion of Single-Walled Carbon Nanotubes: Single Particle Tracking and a Generic Uptake Model for Nanoparticles. *ACS Nano* **2009**, *3*, 149–158.
36. Kostarelos, K.; Lacerda, L.; Pastorin, G.; Wu, W.; Wieckowski, S.; Luangsivilay, J.; Godefroy, S.; Pantarotto, D.; Briand, J. P.; Muller, S. *et al.* Cellular Uptake of Functionalized Carbon Nanotubes Is Independent of Functional Group and Cell Type. *Nat. Nanotechnol.* **2007**, *2*, 108–113.
37. Porter, A. E.; Gass, M.; Muller, K.; Skepper, J. N.; Midgley, P. A.; Welland, M. Direct Imaging of Single-Walled Carbon Nanotubes in Cells. *Nat. Nanotechnol.* **2007**, *2*, 713–717.
38. Cherukuri, P.; Bachilo, S. M.; Litovsky, S. H.; Weisman, R. B. Near-Infrared Fluorescence Microscopy of Single-Walled Carbon Nanotubes in Phagocytic Cells. *J. Am. Chem. Soc.* **2004**, *126*, 15638–15639.
39. Spooner, R. A.; Hart, P. J.; Cook, J. P.; Pietroni, P.; Rogon, C.; Hohfeld, J.; Roberts, L. M.; Lord, J. M. Cytosolic Chaperones Influence the Fate of a Toxin Dislocated from the Endoplasmic Reticulum. *Proc. Natl. Acad. Sci. U.S.A.* **2008**, *105*, 17408–17413.
40. Ludin, B.; Doll, T.; Meili, R.; Kaech, S.; Matus, A. Application of Novel Vectors for GFP-Tagging of Proteins to Study Microtubule-Associated Proteins. *Gene* **1996**, *173*, 107–111.
41. Miyawaki, A. Green Fluorescent Protein-like Proteins in Reef Anthozoa Animals. *Cell Struct. Funct.* **2002**, *27*, 343–347.
42. Hartley, M. R.; Lord, J. M. Cytotoxic Ribosome-Inactivating Lectins from Plants. *BBA-Proteins Proteomics* **2004**, *1701*, 1–14.
43. Roberts, L. M.; Smith, D. C. Ricin: The Endoplasmic Reticulum Connection. *Toxicon* **2004**, *44*, 469–472.
44. Mayerhofer, P. U.; Cook, J. P.; Wahlman, J.; Pinheiro, T. T. J.; Moore, K. A. H.; Lord, J. M.; Johnson, A. E.; Roberts, L. M. Ricin A Chain Insertion into Endoplasmic Reticulum Membranes Is Triggered by a Temperature Increase to 37°C. *J. Biol. Chem.* **2009**, *284*, 10232–10242.
45. Xu, Z. H.; Chen, L. L.; Gu, W. W.; Gao, Y.; Lin, L. P.; Zhang, Z. W.; Xi, Y.; Li, Y. P. The Performance of Docetaxel-Loaded Solid Lipid Nanoparticles Targeted to Hepatocellular Carcinoma. *Biomaterials* **2009**, *30*, 226–232.